Check for updates

New mononuclear Cu(I) compounds: synthesis, characterization, and application to the electroreduction of CO₂†

Alma Arévalo, Enrique Juárez-Francisco, Diego A. Roa, Marcos Flores-Alamo and Juventino J. García [ID] *

This report includes the preparation of a new set of well-defined Cu(I) catalytic precursors of the type [Cu(diphosphine)(PPh₃)NO₃] and [Cu(diphosphine)NO₃], fully characterized by regular analytical methods, including single-crystal XRD (X-ray diffraction). The new compounds were assessed to activate CO_2 in an electrocatalytic process to yield oxalate selectively and with a relatively low overpotential. Some mechanistic insights into this process are also provided; oxalate is a valuable product for further chemical applications.

Introduction

The catalytic conversion of CO_2 to valuable products, such as fuels, commodities, or pharmaceutical chemicals, is a paramount goal to lessen the amount of anthropogenic CO_2, which is one of the leading causes of global warming. The concentration of CO_2 in the atmosphere determined at the Mauna Loa Monitoring Laboratory is reaching 419 ppm (August 2023).[1] This concentration is causing dangerous problems, such as rising sea levels and acidification, effects on biodiversity, and many more environmental issues. Using CO_2 from fossil fuels or industrial waste as a starting material has economic advantages since a costless contaminant can be converted into highly valuable goods,[2] creating a win–win scenario for CO_2 valorization.

Since electrochemical methods can use renewable energy as the driving force for the chemical conversion of substances, acting on a redox-active molecule lowers energy demands like heating. In an electrocatalytic system, the reducing equivalents come directly from the electrode surface as electrons, which are transferred either by diffusion of the catalyst to the electrode surface or by catalyst adsorption onto the electrode surface.[3,4]

To date, there are some reviews about the electroreduction of CO_2 and hydrogen sources to obtain formic acid, hydrocarbons, or alcohols through homogeneous catalysis using different transition metal complexes and typically using Pd, Ir, Ru, and more recently, Ni, Co, or Fe compounds, and macrocyclic ligands or bulky phosphines.[5,6]

Despite the wealth of reports about CO_2 reduction leading to CO and HCO_2H already published, a relatively small amount of them give oxalate as the main product since this involves CO_2 reduction along with a C–C bond formation. Seminal papers by Nonaka[7] describe the production of a mixture of formic acid, oxalic acid, and CO using $CuCl_2$ and PPh_3 with a faradaic efficiency (FE) of 73%. Tanaka[8] outlines the selective oxalate generation in electrochemical CO_2 reduction using triangular metal–sulfide clusters of Ir (FE 60%) and Co (FE 80%). Isobe[9] describes the formation of $C_2O_4^{2-}$ in the electrochemical reduction of CO_2 using $[(Ir(\eta^5\text{-}C_5Me_5))_3(\mu^3\text{-}S)_2](BPh_4)_2$ as a catalytic precursor with a FE of 60%. Another report by Tanaka[10] and coworkers shows the almost selective oxalate formation in electrochemical reduction of CO_2 catalyzed by mono- and di-nuclear $Ru(bpy)_2$ compounds and unsymmetrical chelating ligand complexes that allowed to elucidate the inner sphere mechanism for the formation of oxalate (FE 70%).

Other examples include Jäger[11] with a macrocyclic $[N_4^{2-}]$ Ni: (Ni-Etn-(Me/COOEt)Etn), that is a selective homogeneous catalyst for the electrochemical reduction of CO_2 to oxalate. Wong[12] outlines the use of an iron complex, $[Fe^{II}(dophen)(N\text{-}MeIm)_2]ClO_4$ (N-MeIm = 1-methyl-imidazole), as a catalyst for CO_2 reduction, obtaining a mixture of carbon monoxide, formate and oxalate with a FE of 11%. Bouwman[13] describes a binuclear Cu(I) complex that is oxidized in air by CO_2, giving a tetranuclear Cu(II) complex containing two bridging CO_2-derived oxalate groups, which are precipitated with lithium perchlorate as lithium oxalate, with an efficiency of 96%. Udugala-Ganehenege[14] reports the electrochemistry of a

Facultad de Química, Universidad Nacional Autónoma de México, Circuito Interior, Ciudad Universitaria, Mexico City 04510, Mexico. E-mail: juvent@unam.mx

† Electronic supplementary information (ESI) available: X-ray determinations have been deposited at CCDC with the following numbers: 2314253–2314255. For ESI and crystallographic data in CIF or other electronic format see DOI: https://doi.org/10.1039/d4cy00759j

5394 | *Catal. Sci. Technol.*, 2024, **14**, 5394–5404

This journal is © The Royal Society of Chemistry 2024

hemicyclic Ni(II) complex that showed activity for CO_2 reduction to oxalate, which was detected spectroscopically, but the FE is not disclosed.

The production of oxalate is relevant since it is the main component of lithium batteries (as lithium oxalate[15]) or derived to oxalic acid to be used as a solid lubricant for the separation/recovery of rare earth elements, metal treatment, bleaching agents,[16] textile treatment, leather tanning, marble polishing or as an intermediate of pharmaceuticals or even as medicaments,[17] agrochemicals and in organic synthesis.[18] Some of the metals used are expensive (Ir and Rh), although they produce oxalate in good yields; the cobalt cluster has a high FE, but so far, Fe and Ni are not suitable catalysts for this process; they have low FE. Regarding earth-abundant metals, copper catalysts give the best FE, have low toxicity to humans, and are not expensive.

Considering the above, we turned our attention to the electroreduction of CO_2 using Cu(I) catalysts that selectively produce oxalate in good yields at low overpotential, which is reported herein, along with the synthesis and characterization of four new copper compounds, three of them containing the fragment $R_2P(CH_2)_2$–PR_2, where R = ^iPr (dippe), R = Ph (dppe), R = ethyl (depe); and a closely related complex with 1,1-bis(diisopropylphosphino)ferrocene (dipf).

The different phosphine ligands (P-donor) were selected in the catalyst design based on their electronic (strong σ-donor abilities) and steric (strong binding capabilities owing to the chelate effect) properties; similar synthetic reports are known using N- and S-donor ligands.[19,20] Additionally, the dipf ligand was used to investigate if there is any improvement in reactivity due to the presence of two metals, a redox ligand that enhances the copper function of the catalyst. Finally, nitrate was chosen based on its great capacity as a labile ligand to generate a vacant site at the catalyst.

Results and discussion

Synthesis and characterization of [Cu(dippe)(PPh₃)NO₃] (2)

The synthesis of compound (2) is depicted in Scheme 1; dippe,[21] and [Cu(PPh₃)₂(NO₃)][22] were prepared according to the reported methods.

Compound (2) was obtained as a white solid, washed with hexane, then with toluene, and finally dried in vacuum for 4 hours; an isolated yield of 80% was obtained after workup. Suitable single crystals for XRD were obtained for complex (2) from a saturated THF–toluene solution stored at
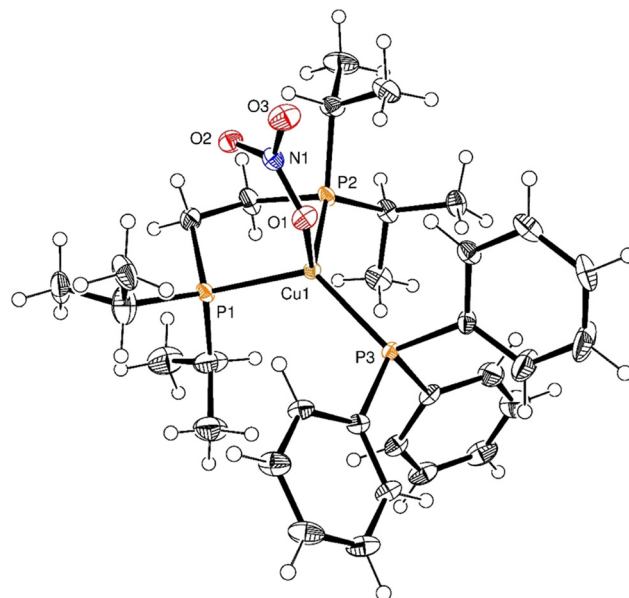

Fig. 1 ORTEP plot (50% probability) for complex (2). Labels of carbon atoms are omitted for clarity.

−30 °C for 48 h in a drybox. The corresponding ORTEP (Oak Ridge Thermal Ellipsoid Program) plot for (2) is depicted in Fig. 1.

Complex (2) is a diamagnetic d^{10} copper(I) complex suitable for NMR (nuclear magnetic resonance) study. The room temperature $^{31}P\{^1H\}$ NMR spectra for (2) displayed two signals at 0.45 ppm (PPh₃) and 12.1 ppm (dippe) (Table 1, entry 1); both signals are broad singlets; thus, the coupling constants cannot be determined. Due to the air sensitivity of the dippe ligand complex, (2) was synthesized under an argon atmosphere; nevertheless, after preparation, (2) turned out to be air-stable as a solid for several days in an uncontrolled atmosphere; however, solutions of (2) are not stable and change from colorless to blue, characteristic of copper(II) compounds.

As expected, upon coordination with the copper center, the chemical shift corresponding to each P-donor ligand moves to a lower field (Scheme 2). The $^{13}C\{^1H\}$ spectra of (2) show three singlets at the aliphatic region corresponding with the chelate phosphine and four signals for the aromatic rings of the PPh₃ moiety. The signal at δ = 137.81 ppm corresponds to the *ipso* carbon of the phosphine phenyl ring, as shown in Fig. S4.†

The IR (ATR-neat) data for the nitrate moiety of the new copper compounds are listed in Table 2.

Suitable single crystals for XRD were also obtained for complex [Cu(depe)(PPh₃)NO₃] (3) and [Cu(dipf)NO₃] (5) from saturated THF–hexane solutions stored at −30 °C under an argon atmosphere. The corresponding ORTEP plot for (3) is depicted in Fig. 2, and the ORTEP plot for (5) is in Fig. 3.

The XRD studies for (2), (3) and (5) complexes show that the copper atom is in a tetracoordinate environment. This coordination is frequently found in Cu(I) complexes; however,
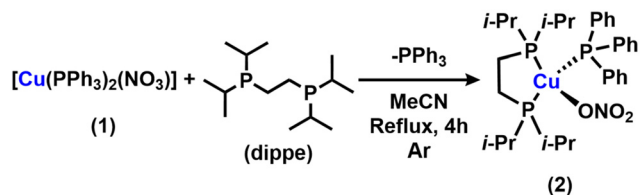

Scheme 1 Synthesis of [Cu(dippe)(PPh₃)NO₃] (2). Compounds **3**, **4**, and **5** were prepared similarly.

This journal is © The Royal Society of Chemistry 2024

Catal. Sci. Technol., 2024, **14**, 5394–5404 | **5395**

Table 1 Relevant δ_P values for the new copper compounds in THF-d_8 at 25 °C (operating at 242.9 MHz for $^{31}P\{^1H\}$)

Entry	Complex	PPh$_3$ δ_P (ppm)	Biphosphine δ_P (ppm)
1	[Cu(dippe)(PPh$_3$)NO$_3$] (**2**)	0.45	12.1
2	[Cu(depe)(PPh$_3$)NO$_3$] (**3**)	4.45	−4.5
3	[Cu(dppe)(PPh$_3$)NO$_3$] (**4**)	2.87	−6.25
4	[Cu (dipf)NO$_3$] (**5**)	—	3.13
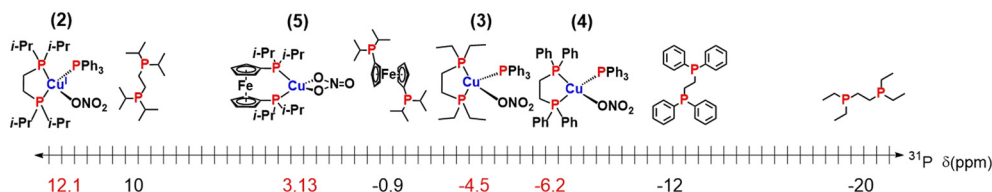
Scheme 2 δ_P values for copper compounds vs. δ_P for free diphosphines dippe, dppe,[23] depe,[24] and dipf,[25] (PPh$_3$ excluded).

this is the first report of the [Cu(dippe)(PPh$_3$)NO$_3$] (**2**), [Cu(depe)(PPh$_3$)NO$_3$] (**3**) and [Cu(dipf)NO$_3$] (**5**) crystal structures. Table 3 shows selected bond lengths [Å], angles [°], and torsion angles [°]. The sum of the internal bond angles[26] centered at copper is 656.77° for (**2**), 657.08° for (**3**), and 643.09° for (**5**), and the tau(4)-descriptor for 4-coordination (τ_4) values[27] of 0.78 and 0.81 are evidence that (**2**) and (**3**) are close to the trigonal pyramidal geometry (TRP), while (**5**) shows a perfect TRP geometry with τ_4 of 0.85. The puckering parameters of the five membered ring Cu(1)–P(1)–C(1)–C(2)–P(2) in (**2**), with $Q(2) = 0.454$ Å and $\varphi(2) = 250.5(2)°$, establish the closest pucker descriptor being enveloped on C1; while the same analysis for (**3**) results in $Q(2) = 0.456$ Å and $\varphi(2) = 278.9(3)°$ that corresponds to a closest pucker descriptor being twisted on C(1)–C(2).

For compound (**2**), probably the isopropyl group has a higher steric effect with triphenylphosphine, resulting in longer Cu(1)–P(1) and Cu(1)–P(2) bond distances (approx. 2.294 Å) compared to the average value reported (2.273 Å) at the Cambridge Crystallographic Data Centre (CCDC-2023). For compound (**3**), the distance Cu(1)–P(1) is almost identical to the average value reported (2.273 Å) in CCDC-2023. In both compounds, the oxygen atom of the nitrate group is bonded in a κ^1-O coordination mode. In compound (**5**), the presence of the ferrocenyl group bonded between P(1) and P(2) opens the angle P(1)–Cu(1)–P(2), and increases the distance between the P atoms to 3.83 Å, causing a decrease in the Cu(1)–P distances to a value of 2.23 Å, similar to the average Cu–P value reported in the CDCD-2023 for P as a monodentate ligand. Additionally, the steric effects of ferrocene avoid the

coordination of triphenylphosphine and favor the nitrate group to act as a bidentate κ^2-O ligand to copper. Note that there is no interaction between the Fe and Cu atoms in (**5**). Selected bond lengths [Å] and angles [°] for (**2**), (**3**) and (**5**) are shown in Tables S2, S4, and S6,† respectively.

Electrochemical studies

All the experiments reported here were done in an airtight, undivided glass cell equipped with a gas inlet and outlet to pass argon or CO$_2$ through the solution. A three-electrode system was used during the experiments. The working electrode was always glassy-carbon. The counter electrode was a Pt wire. The pseudo-reference electrode was a silver

Table 2 νN–O values for the copper(ı) catalysts (cm^{-1})

Entry	Complex	NO sym.	NO asym.
1	[Cu(dippe)(PPh$_3$)NO$_3$] (**2**)	1299	1399
2	[Cu(depe)(PPh$_3$)NO$_3$] (**3**)	1297	1434
3	[Cu(dppe)(PPh$_3$)NO$_3$] (**4**)	1274	1434
4	[Cu (dipf)NO$_3$] (**5**)	1286	1431
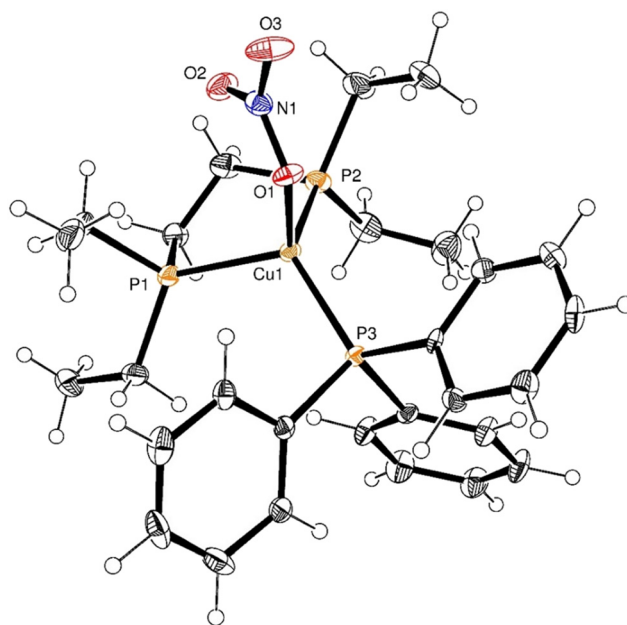
Fig. 2 ORTEP plot (50% probability) for complex (**3**). Labels of carbon atoms are omitted for clarity.

5396 | *Catal. Sci. Technol.*, 2024, **14**, 5394–5404

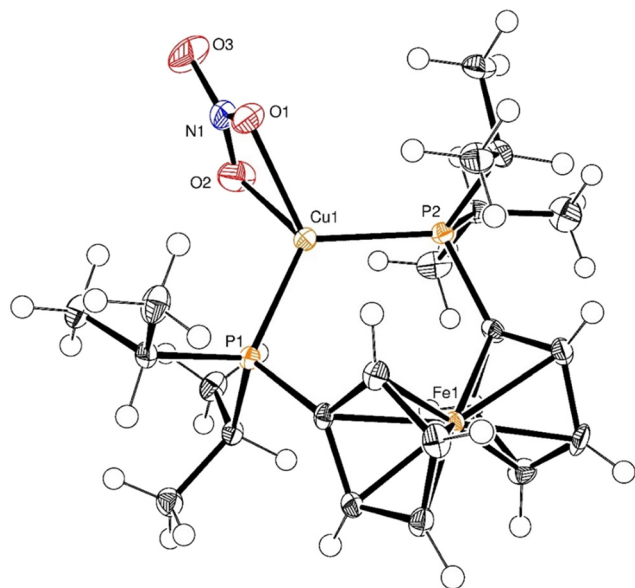This journal is © The Royal Society of Chemistry 2024

Fig. 3 ORTEP plot (50% probability) for complex (**5**). Labels of carbon atoms are omitted for clarity.

wire in a small glass tube fitted with a Vycor™ membrane and filled with an electrolyte solution that was internally referenced with a ferrocene/ferrocenium pair. 10 mL of 0.1 M TBAPF$_6$ (tetrabutylammonium hexafluorophosphate) in acetonitrile (MeCN) was used as the supported electrolyte. The Cu(I) catalyst concentration used was 10^{-3} M. The reaction was done using dry MeCN as a solvent, so a broader potential window for the experiment and a higher CO$_2$ solubility was achieved. The procedure described here is the same for all the copper complexes reported in this work. Cyclic voltammogram (CV) plotting follows the IUPAC (International Union of Pure and Applied Chemistry) convention. To discard the contribution of heterogeneous species such as metallic Cu(0), the rinse test after cathodic scanning was made.

Electrochemistry under an argon atmosphere of Cu(I) complexes.

Electrochemical studies, including CV determination ranging from −3.093 to 1.407 V vs. Fc after the electrolyte solution had been bubbled with argon for 10 minutes, are shown in Fig. 4. When scanning a solution of complex (**2**) towards the cathode potential, it can be observed that the complex has one reduction peak at −3.01 V vs. Fc that was assigned to the reduction process Cu(I)/Cu(0). Three anodic peaks correspond to the phosphine oxidation process, L$_1$ corresponds to the oxidation process of dippe, and L$_2$ corresponds to PPh$_3$ oxidation, as shown in Fig. 4. The corresponding CV curves for the phosphine ligands leading to this assignment are at Fig. S28–S31.†

This study was performed at different scanning rates, and no additional oxidation or reduction peaks were observed (Fig. S32 and S33†). A similar study was assessed for all the copper complexes used here; the reduction values for Cu(I)/Cu(0) are somewhat similar and are summarized in Table 4.

Electrochemistry under a CO$_2$ atmosphere of Cu(I) complexes

The electrolytic behavior for CO$_2$ reduction of compound (**2**) was assessed under a CO$_2$ atmosphere by carrying out CV experiments on a glassy carbon (GC) electrode; it was found that the CV plot in the CO$_2$ atmosphere displays an enhanced irreversible reduction wave at −3.07 V compared with the plot obtained under an Ar atmosphere at the same scanning rate, this value is the E_{cat}^0 of the system; at this potential, a substantial current increase was observed, related to a reduction process taking place between CO$_2$ and the catalyst (i_{cat}). Again, this study was repeated at different scanning rates, and no new peaks were observed (Fig. S34 and S35†).

Electrochemistry with proton sources

The study presented here was done under aprotic conditions; the solvent was chosen due to a broader potential window and a higher CO$_2$ solubility (0.28 M).[28] Thus, the electrocatalytic CO$_2$

Table 3 Selected bond lengths [Å], angles [°], and torsion angles [°] for compounds **2**, **3**, and **5**

| 2		3		5	
Bond	[Å]	Bond	[Å]	Bond	[Å]
Cu(1)–O(1)	2.146(2)	Cu(1)–O(1)	2.090(3)	Cu(1)–O(1)	2.1598(15)
Cu(1)–P(1)	2.2944(9)	Cu(1)–P(1)	2.2759(16)	Cu(1)–P(1)	2.2305(6)
Cu(1)–P(2)	2.2904(9)	Cu(1)–P(2)	2.2593(16)	Cu(1)–P(2)	2.2383(6)
Cu(1)–P(3)	2.2688(9)	Cu(1)–P(3)	2.2323(13)	Cu(1)–O(2)	2.2580(16)
Angle	[°]	**Angle**	[°]	**Angle**	[°]
O(1)–Cu(1)–P(3)	97.27(7)	O(1)–Cu(1)–P(3)	99.13(10)	O(1)–Cu(1)–P(1)	122.00(5)
O(1)–Cu(1)–P(2)	111.01(7)	O(1)–Cu(1)–P(2)	109.20(11)	O(1)–Cu(1)–P(2)	113.29(4)
P(3)–Cu(1)–P(2)	124.54(3)	P(3)–Cu(1)–P(2)	129.28(6)	P(1)–Cu(1)–P(2)	117.96(2)
O(1)–Cu(1)–P(1)	108.62(7)	O(1)–Cu(1)–P(1)	112.16(11)	O(1)–Cu(1)–O(2)	58.44(6)
P(3)–Cu(1)–P(1)	125.08(3)	P(3)–Cu(1)–P(1)	116.47(6)	P(1)–Cu(1)–O(2)	117.31(4)
P(2)–Cu(1)–P(1)	90.25(3)	P(2)–Cu(1)–P(1)	90.84(5)	P(2)–Cu(1)–O(2)	114.09(5)
Torsion angles	[°]	**Torsion angles**	[°]	**Torsion angles**	[°]
P(1)–Cu(1)–O(1)–N(1)	60.1(2)	P(1)–Cu(1)–O(1)–N(1)	−61.1(3)	P(1)–Cu(1)–O(1)–N(1)	−106.60(11)
P(2)–Cu(1)–O(1)–N(1)	−37.6(2)	P(2)–Cu(1)–O(1)–N(1)	38.0(3)	P(2)–Cu(1)–O(1)–N(1)	102.84(12)
P(3)–Cu(1)–O(1)–N(1)	−169.0(2)	P(3)–Cu(1)–O(1)–N(1)	175.3(3)	P(1)–Cu(1)–O(2)–N(1)	114.57(12)
O(2)–N(1)–O(1)–Cu(1)	−19.4(4)	O(2)–N(1)–O(1)–Cu(1)	11.1(6)	P(2)–Cu(1)–O(2)–N(1)	−101.44(12)

Paper
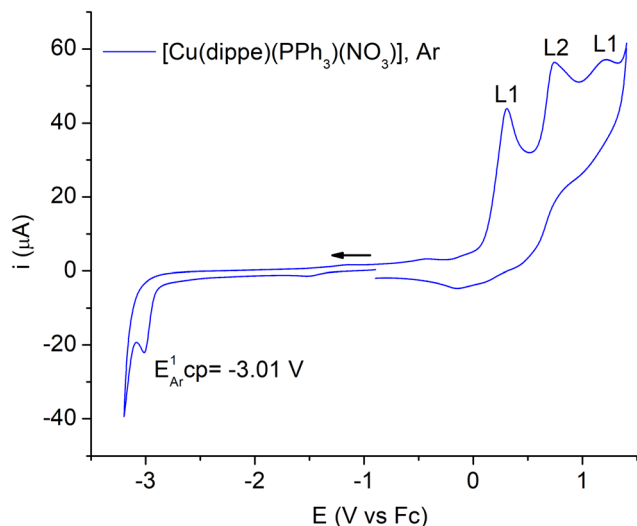
Fig. 4 CV of complex (**2**) under an Ar atmosphere.

Table 4 Cathodic peaks of the Cu(I) complexes under an Ar atmosphere

Compound	$E_{Ar}^{Cu(I)/Cu(0)}$ (V $vs.$ Fc)
[Cu(PPh$_3$)$_2$NO$_3$] (**1**)	−2.44
[Cu(dippe)(PPh$_3$)NO$_3$] (**2**)	−3.01
[Cu(depe)(PPh$_3$)NO$_3$] (**3**)	−2.89
[Cu(dppe)(PPh$_3$)NO$_3$] (**4**)	−2.97
[Cu (dipf)NO$_3$] (**5**)	−2.91

reaction shown was assessed in the presence of various proton donors with different pK_a values added into the system to explore the potential formation of protonated products or the hydrogen evolution reaction (HER). The results are summarized in Table 5.

As seen in Table 5, all the tested proton sources favored the HER process; the more acidic substances showed the best HER activity (PTSA and PhCO$_2$H), and two showed modest HER activity (AcOH and PhOH), as shown in Fig. S36–S66.† However, using a proton source for the CO$_2$RR (electrochemical reduction of carbon dioxide), the catalytic current (i_{cat}) was diminished compared with the i_{cat} obtained without a proton source, as seen in Fig. 6.

Since the CO$_2$ reduction proceeds under aprotic conditions (*vide supra*), one of the possible outcomes is the oxalate formation[11,13] (the other one, disproportionation to

Table 5 HER activity with the different substances investigated. pK_a values are reported in acetonitrile[29] (green mark= HER, red mark= negative result)

Acid	pK_a	(**2**)	(**3**)	(**4**)	(**5**)	(**1**)
PTSA	9.97	✔	✔	✔	✔	✔
PhCO$_2$H	21.5	✔	✔	✔	✔	✔
AcOH	23.5	✘	✔	✘	✘	✔
PhOH	29.2	✘	✔	✘	✘	✘

Table 6 Cu(I)–O bond distances of Cu(I) compounds

Compound	Cu(I)–O (Å)
(**2**)	2.1416
(**3**)	2.09
(**5**)	2.1498, 2.2580

CO and carbonate was not observed) by a two electron process:[30]

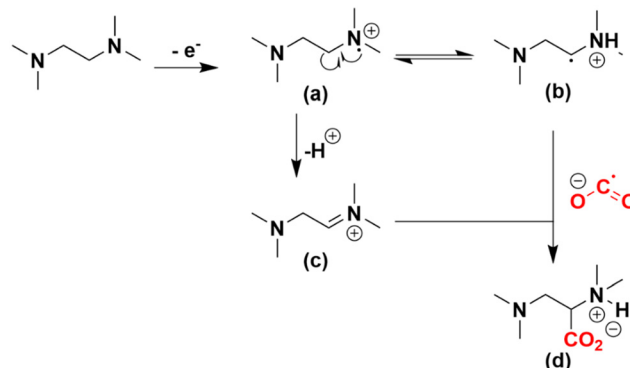$$2CO_2 + 2e^- \xrightarrow{\text{catalyst}} C_2O_4{}^{2-}$$
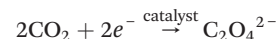
To corroborate the oxalate formation, a solution of CaCl$_2$ was added to the electrochemical mixture, and a white solid was immediately formed, filtered, washed with water, and dried under vacuum before being analyzed. IR-ATR (infra-red attenuated total reflection) confirmed the white solid as calcium oxalalate, as shown in Fig. 7.

Mechanistic proposal

It is known that the one-electron reduction of CO$_2$ to form the CO$_2$$^{•-}$ radical anion needs a big overpotential, −1.99 $vs.$ NHE,[32] due to an internal reorganization of CO$_2$ from a linear molecule to a bent one to interact with the catalyst. Oxalate formation from CO$_2$ electroreduction has a negative redox potential of E^0(CO$_2$/CO$_2$$^{•-}$) at −1.96 V $vs.$ NHE.[33] Our findings in this work show an overpotential of −0.39 V $vs.$ NHE, which energetically is more favorable for the CO$_2$RR to oxalate.

The following experiments were done to shed some light on the catalytic cycle. From the previously discussed experiments, it seems that the active species was a Cu(0) catalyst; thus, complex (**2**) reacted with sodium-amalgam[34] to reduce Cu(I); the Cu(0) intermediate is a paramagnetic intermediate subjected to an EPR spectroscopic study ($I = 3/2$), where the corresponding spectra are shown in Fig. 8. The $g = 2.0012$ agrees with closely related Cu(0) compounds[35] and confirms a one-electron reduction process; when CO$_2$ is added to the EPR tube, the signal corresponding to copper (0) is not observed due to the oxidation to the Cu(I) complex (red line, Fig. 8).

Scheme 3 Proposed mechanism for the formation of (d).

5398 | *Catal. Sci. Technol.*, 2024, **14**, 5394–5404

This journal is © The Royal Society of Chemistry 2024

Regarding the nitrate moiety, it displays the κ^1-O for (2) and (3) coordination and κ^2-O for compound (5); it is known that nitrate is a weak ligand to Cu(ɪ) which is confirmed by the Cu(ɪ)–ONO$_2$ bond distances obtained from the XRD data of the compounds reported here (Table 6), and these bond distances are longer compared to other complexes reported elsewhere,[36] for instance, a Cu–O bond distance on copper nitrate[37,38] (1.973 Å, average). These data support that the nitrate group generated in the current report may be prone to dissociate allowing a CO$_2$ molecule to be coordinated and reduced, allowing for an inner sphere mechanism.

During the CPC experiment described before, the released gases were bubbled in a suspension of 20 mg of Wilkinson catalyst in 5 mL of ethanol.[39] The color of the suspension changed from brick-red to a dark yellow precipitate. The IR (ATR) spectra of the solid (Fig. 9) showed a signal at 1655 cm^{-1} assigned to an N–O bent fragment,[40] and the elemental analysis agrees for [Rh(PPh$_3$)$_3$Cl(NO)] (C$_{54}$H$_{45}$ONP$_3$ClRh): %C, 67.89, %H, 4.75, %N, 1.46. Found: %C, 67.78, %H, 5.23, %N, 1.47. Fig. S67.†

To investigate if triphenylphosphine has any effect on the system at hand, a CV was done by adding 0.5 equivalents of PPh$_3$; the test showed that PPh$_3$ slightly inhibits the cathodic current of the process (Fig. 10).

To verify the CO$_2$$^{•-}$ formation, a CPC experiment was done under the same conditions described before, but 10 eq. of TMEDA were added to the matrix cell; at the end of the test, a GC–MS of the solution was obtained, and product (d), as shown in Scheme 3, was detected (Fig. S68†).

It is well known that aliphatic amines generate radical cations.[41,42] An initial electron transfer occurs to obtain species (a), which is in equilibrium with (b), then (a) loses a proton and forms the imidium salt (c); finally (b) or (c) can react with the CO$_2$$^{•-}$ formed during the experiment at the cathode to yield (d), and the protonated species (d) may trap back H$^+$ from the media. The addition of CO$_2$$^{•-}$ to double bonds has been previously reported,[43] and such additions are common in free radical chemistry, Fig. S68.†

Considering the findings of the current report and a recent publication,[44] the following simplified catalytic cycle is proposed as shown in Fig. 11.

The original Cu(ɪ) complex is reduced to form a Cu(0) intermediate, then a reaction with CO$_2$ occurs to produce a CO$_2$ adduct, allowing for one-electron reduction to form the CO$_2$$^{•-}$ radical that dimerizes to yield oxalate.

Faradaic efficiency (FE)

To assess the stability of the catalyst, to study the products obtained during the experiment, and also to establish the faradaic efficiency of the system, controlled potential coulometry (CPC) was performed at −3.1 V *vs.* Fc, in 1 h, which was found to be 40.2% calculated according to the reported methods,[46,47] as shown in Fig. 12.

TOF determination

The turnover frequency (TOF) in the context of homogeneous electrocatalysis refers only to the activity of catalyst molecules present in the reaction–diffusion layer close to the electrode surface and independent of the total amount of the catalyst contained in the electrolyte,[6] so that the TOF is a function of the applied potential. To calculate this value, it is necessary to know the value of k_{app} (the overall rate of the homogeneously catalyzed reaction); this value was calculated according to Dempsey.[48]

In the current report, a typical S shape wave was not observed; therefore, an analysis of the onset of the catalytic current can be used by applying the FOWA (foot-of-the-wave-analysis) standard to determine k_{app} (apparent rate constant) using the CV traces obtained. Thus, the appropriate process for this case begins with the obtention of the value of i/i_p:
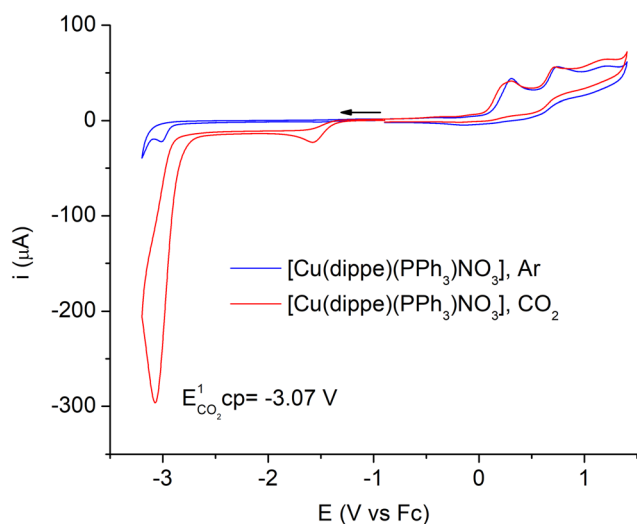

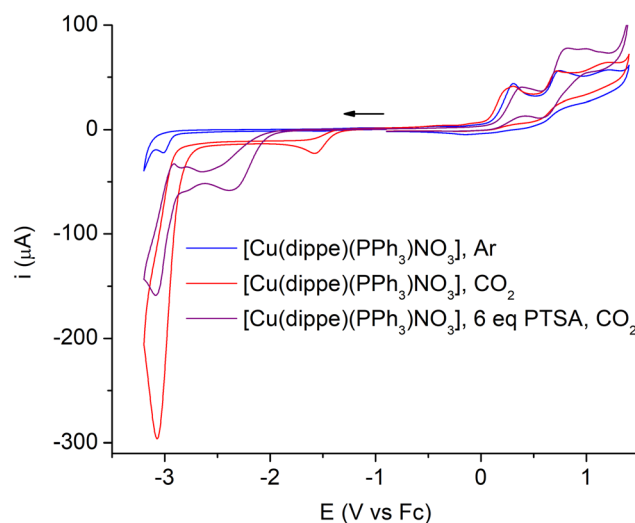Fig. 5 CV of complex (2) under a CO$_2$ atmosphere.

Fig. 6 Inhibition of the CO$_2$RR process in the presence of proton sources (red line cathodic peak, 274.21 μA, purple line cathodic peak with PTSA, 136.55 μA).
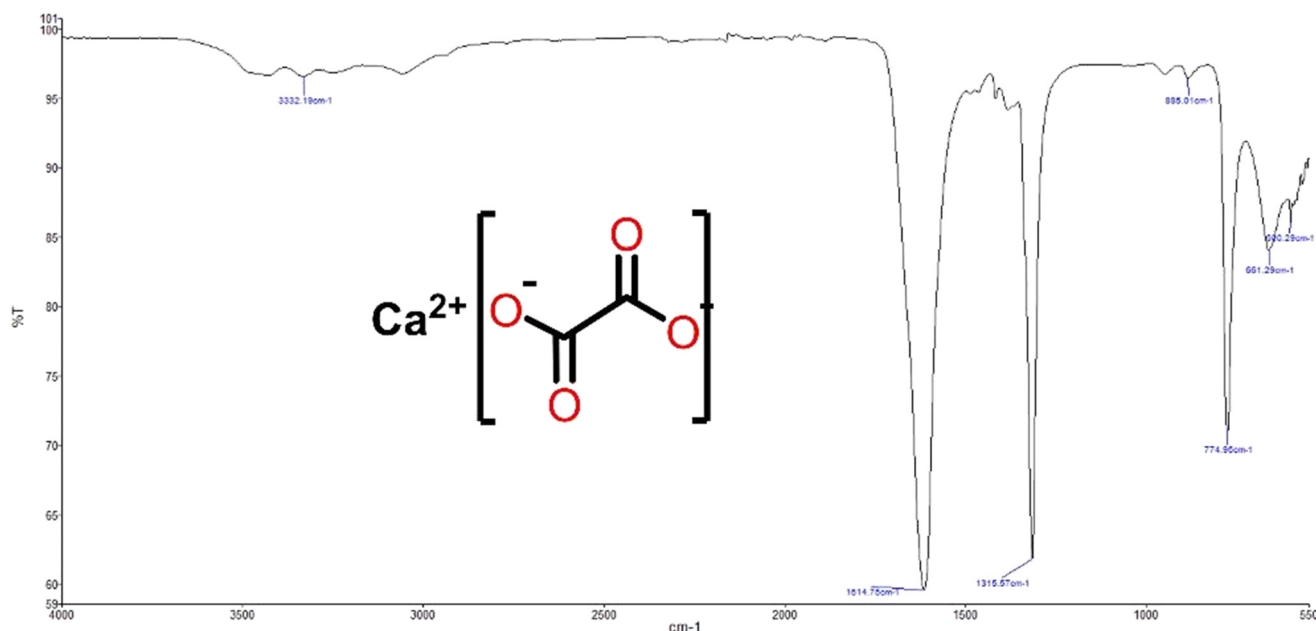
This journal is © The Royal Society of Chemistry 2024

Catal. Sci. Technol., 2024, **14**, 5394–5404 | **5399**

Fig. 7 IR (ATR) of calcium oxalate obtained from the CPC experiment of complex (**2**).[31]

$$\frac{i}{i_p} = \frac{2.24\sqrt{\frac{RT}{n\,Fv}}\sqrt{n'k_{app}}}{1 + \exp\left[\frac{nF}{RT}(E - E_{redox})\right]} \quad (1)$$

E_{Redox}: half wave catalyst reduction potential under Ar: -2.97 V (Fig. 4).

i_P: catalyst maximum cathodic current without substrate: 22.1053 microA. (Fig. 4).

i: current obtained from CV (Fig. 5).

n: number of transferred electrons from the electrode to the catalyst: **1**.

R: ideal gases constant, 8.314 J K^{-1} mol^{-1}.

T: working temperature (K), 298.15 K.

F: Faraday constant, 96 485 C mol^{-1}.

Fig. 8 EPR experiments for compound (**2**).

κ_{app}: as described (*vide infra*).

v: working sweep speed: 0.1 V s^{-1}.

n': catalyst mole number for interchange and product formation: **1**.

Then, a graph with coordinates $y = i/i_p$ and $x =$ eqn (1) is obtained (see Fig. 13); from the slope (m) the value of k_{app} is obtained according to eqn (2):

$$k_{app} = \frac{m^2}{(2.24)^2\left(\frac{RT}{n\,Fv}\right)n'} \quad (2)$$

where $m =$ slope (from Fig. 13).

To calculate the TOF value for complex (**2**), the following equation was used.[49]

$$TOF = \frac{k_{app}}{1 + \exp\left[\frac{F}{RT}\left(E^\circ_{A/P} - E_{cat}\right)\right] \times \exp\left(-\frac{F}{RT}\eta\right)} \quad (3)$$

$E^\circ_{cat} = -2.38$ V *vs.* NHE.

$R = 8.314$ J K^{-1} mol^{-1}.

$T = 298.15$ K.

$F = 96 485$ C mol^{-1}.

$E^\circ_{A/P} = -1.99$ V *vs.* NHE.

$\eta = 0.39$ V.

The values obtained for the CO$_2$RR cathodic process are from Fig. 5.

From Fig. 13, a slope value of 19.984 is obtained, then using that in eqn (2), $k_{app} = 309.8$ s^{-1}. Finally, from eqn (3), the TOF value for complex (**2**) is 154.9 s^{-1}. For the other Cu(I) complexes, (**3**), (**4**), and (**5**), since all of them exhibited the same behavior and the same E°_{cat} potential value (-3.0 V *vs.* Fc, average) giving oxalate as product, the study was limited to complex (**2**) due to this compound had the higher i_{cat} value; see the ESI.†
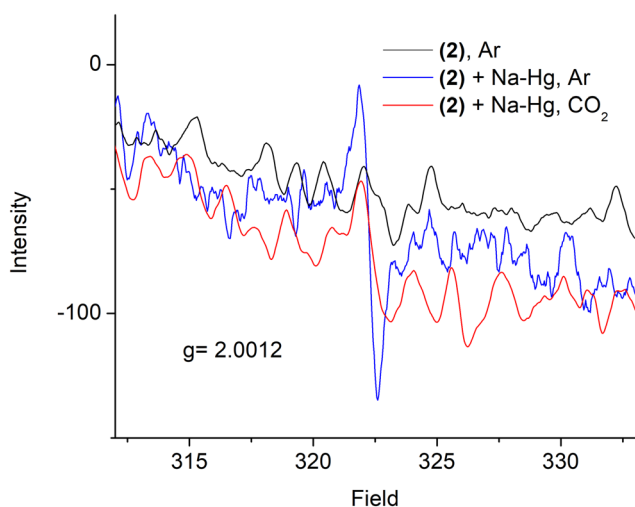
5400 | *Catal. Sci. Technol.*, 2024, **14**, 5394–5404

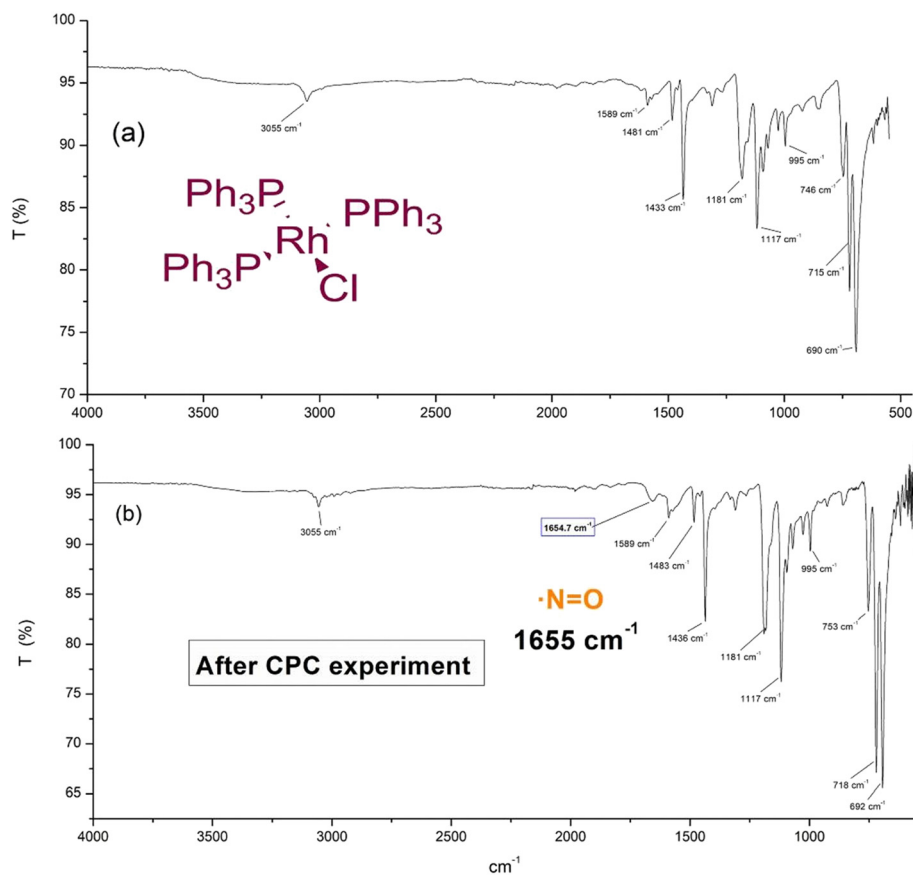This journal is © The Royal Society of Chemistry 2024

Fig. 9 (a) IR (ATR) of the Wilkinson catalyst. (b) IR-ATR after CPC experiment, NO bent v = 1655 cm^{-1}.[40]

Conclusions

Four new well-defined Cu(I) complexes [Cu(diphosphine)(PPh$_3$) NO$_3$], diphosphine = dippe, depe, and dppe, and complex [Cu(dipf)NO$_3$] were synthesized and fully characterized, including single crystal X-ray structures. Complex (**2**) showed good activity for the CO$_2$RR, giving oxalate as a product selectively at room temperature, with a good yield and a low overpotential (0.39 V). Oxalate production is relevant due to their variety of applications, such as energy storage in lithium-ion batteries, due to their high energy density and long lifetime.[50]

Experimental section

General considerations

Unless otherwise noted, all manipulations were performed under an argon atmosphere in an MBraun glove box (<1 ppm H$_2$O and O$_2$) or using standard Schlenck techniques.
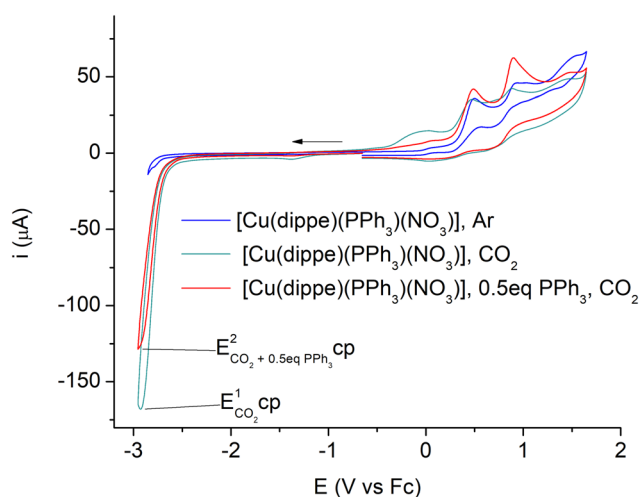

Fig. 10 CV of complex (**2**) and 0.5 eq. of PPh$_3$.
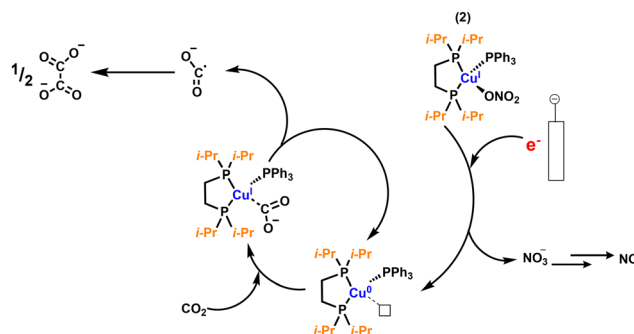
Fig. 11 Proposed catalytic cycle for the CO$_2$RR to oxalate.[45]

This journal is © The Royal Society of Chemistry 2024

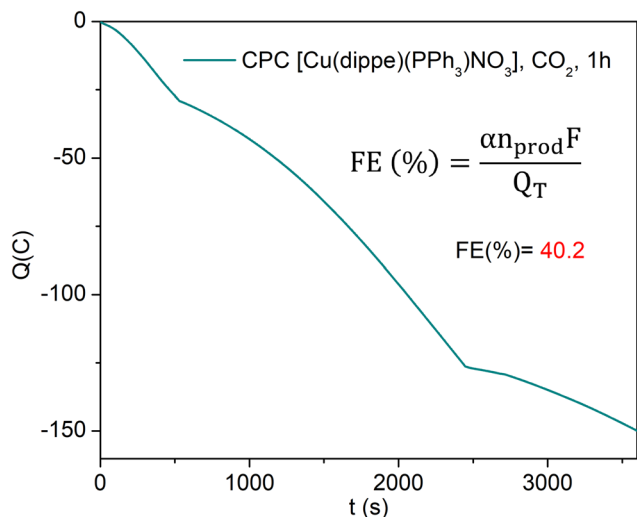Catal. Sci. Technol., 2024, **14**, 5394–5404 | **5401**

Fig. 12 CPC for the CO_2 reduction using (**2**). Electron number interchanged ($\alpha = 2$); n_{prod} (3.435×10^{-4}), F (Faraday constant). Total charge (Q_T, 149.9 C).

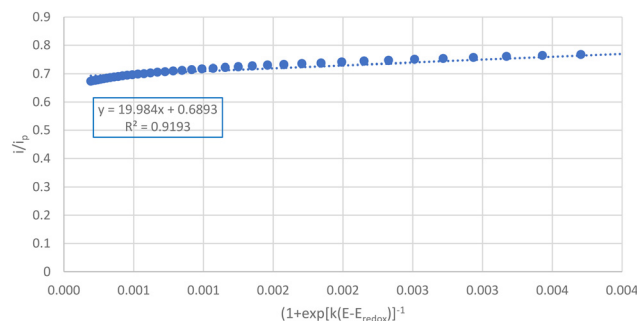**Fig. 13** Graph where $y = i/i_p$ and $x =$ eqn (1).

The phosphine compounds, tristriphenylphosphine (PPh_3), ethylenebis(diphenylphosphine) (dppe), 1,2-bisethylene(diethylphosphino) (depe), 1,1'-bis(diisopropylphosphine)ferrocene (dipf) and $Cu(SO4)_2$ trihydrate were purchased from Aldrich; 1,2-bis(diisopropylphosphino)ethane (dippe) was synthesized as reported.[21] Nitratobis(triphenylphosphine)copper(I) (**1**) was synthesized as stated by Gysling, H. J.[22] Acetonitrile was dried and distilled from CaH_2 (Aldrich), toluene was dried and distilled from sodium, and hexanes were dried in an MBraun solvent purification system (MB-SPS). All substances were reagent grade. Deuterated solvents for NMR experiments were purchased from Aldrich and stored over 3 Å molecular sieves in the glove box. All NMR spectra of complexes and products were recorded on a 600 MHz Varian Unity spectrometer. NMR determinations for air-sensitive samples were collected using a sealed J. Young NMR tube. The ^1H (600 MHz), $^{13}C\{^1H\}$ (150.9 MHz) and $^{31}P\{^1H\}$ (242.9 MHz) were obtained from solutions in THF-d_8 unless otherwise stated. ^1H and ^{13}C NMR chemical shifts δ (ppm) are reported relative to the residual proton

resonance in the deuterated solvent. $^{31}P\{^1H\}$ spectra are reported relative to external 85% H_3PO_4. GC–MS determinations were performed using an Agilent 5975C instrument with a 30 m DB-5MS capillary (0.32 mm i.d.) column. Electrochemical studies were carried out using a Gamry Instruments-Eurocel potentiostat. CPC experiments were done with an isolated platinum wire in a small glass tube fitted with a Vycor™ membrane and filled with the electrolyte solution. All of the electrochemical experiments were made in CH_3CN.

The following describes a particular procedure, but it was observed as a general methodology for all used substrates in terms of the use of the same molar ratios between the substrate and dippe, dppe, depe and 1,1'-bis(di-isopropylphosphine)-ferrocene.

Synthesis of compound (**2**)

To a solution of compound (**1**) (0.39 g, 5.9×10^{-4} mol) in 4 mL of MeCN, a solution of dippe (0.16 g, 5.9×10^{-4} mol) in 4 mL of MeCN was added at room temperature. Then, the solution was heated at 70° for 3 h under an argon atmosphere. At the end of the reaction time, 10 mL of hexane is added, and a white solid is obtained, which is filtered and then washed with toluene. The white solid is dried in the vacuum line for 4 h. Yield 80%.

Compounds (**3**) and (**4**) were synthesized as described with depe and dppe, respectively. For (**5**), the dipf was added as a yellow suspension.

Spectroscopic and analytic details

Compound (**2**). NMR (600. MHz): $^{31}P\{^1H\}$ (THF-d_8), $\delta = 0.45$ ppm (s, PPh_3), $\delta = 12.14$ ppm (s, dippe). $^{13}C\{^1H\}$ $\delta = 20.21$ ppm (s, –CH_3), $\delta = 20.53$ ppm (s, –CH_2-bridge), $\delta = 25.18$ ppm (s, –CH-^iPr), $\delta = 129.7$ ppm (d, m-PPh_3, $^3J_{C–P} = 7.5$ Hz), $\delta = 130.6$ ppm (s, p-PPh_3), $\delta = 135.5$ ppm (d, o-C–PPh_3, $^2J_{C–P} = 15.09$ Hz), $\delta = 137.81$ ppm (s, ^iC–PPh_3).

^1H, $\delta = 1.20$ ppm (s, –CH_3), $\delta = 1.91$ ppm (s, –CH_2-bridge), $\delta = 2.15$ ppm (s, –CH–isopropyl), $\delta = 7.37$ ppm (m, H_o y H_m –PPh_3), $\delta = 7.54$ ppm (t, H_p –PPh_3). IR (ATR-neat): 3055 cm^{-1}, 2954 cm^{-1}, 2868 cm^{-1} (w, C≡C –PPh_3 ring), 1399 cm^{-1} (s, N–O sym), 1299 cm^{-1} (s, N–O asymm.), 700 cm^{-1} (s, –PPh_3 ring). Anal. Calcd. for: $C_{32}H_{47}O_3NP_3Cu$: %C, 59.11, %H, 7.3, %N, 2.15. Found: %C, 56.9, %H, 7.5, %N: 2.3. Melting point: 202 °C (d).

Compound (**3**). [(depe)Cu(PPh_3)NO_3]. NMR (600 MHz): $^{31}P\{^1H\}$ (THF-d_8): $\delta = -4.5$ (d, P–diphosphine), $\delta = 4.4$ ppm (m, –PPh_3). ^1H: $\delta = 0.97$ ppm (m, –CH_3), $\delta = 1.63$ ppm (m, –CH_2), $\delta = 2.54$ ppm (m, –CH_2 bridge), $\delta = 7.39$ ppm (m, m-PPh_3), $\delta = 7.44$ ppm (m, o-PPh_3), $\delta = 7.54$ ppm (ws p-PPh_3), $^{13}C\{^1H\}$, $\delta = 9.28$ ppm (s, –CH_3), $\delta = 17.87$ ppm (s, –CH_2–), $\delta = 23.26$ ppm (s, –CH_2-bridge), $\delta = 130.03$ ppm (m, m-PPh_3), $\delta = 131.22$ ppm (ws, p-PPh_3), $\delta = 135.36$ ppm (d, o-PPh_3, $J = 15.09$ Hz). IR (ATR-neat): 3053–2875 cm^{-1} (–CH_3 and –CH_2–, str.), 1434 cm^{-1} (N–O asym), 1337 cm^{-1} (C–H felx.), 1297 cm^{-1} (N–

5402 | *Catal. Sci. Technol.*, 2024, **14**, 5394–5404

This journal is © The Royal Society of Chemistry 2024

O sym), 1090–1028 cm^{-1} (C–H arom.), 694 cm^{-1} (C–H arom.). Anal. Calcd. for $C_{28}H_{39}O_3NP_3Cu$: %C, 56.7, %H, 6.62, %N, 2.3. Found: %C, 55.5, %H, 6.7, %N, 2.41. Melting point: 257 °C (d).

Compound (**4**). NMR (600 MHz): $^{31}P\{^1H\}$ (THF-d_8): δ = −6.22 ppm (s, P-bridge), δ = 2.91 ppm (m, –PPh$_3$). ^{1}H: δ = 2.42 ppm (m, –CH-bridge), δ = 7.22–751 ppm (m, aromatic phosphines). IR (ATR-neat): 3052 cm^{-1} (C–H str. arom.), 1434 cm^{-1} (N–O asym), 1274 cm^{-1} (N–O sym), 1096–1022 cm^{-1} (C–H arom.), 692 cm^{-1} (C–H arom.). Anal. Calcd. for $C_{44}H_{43}O_3$-NP_3Cu: %C, 66.8, %H, 5.4, %N, 1.8. Found: %C, 66.8, %H, 5.1, %N, 2.6. Melting point: 256 °C (d).

Compound (**5**). NMR (600 MHz): $^{31}P\{^1H\}$ (THF-d_8), δ = 3.13 ppm (s). ^{1}H, δ = 1.30 ppm (m, –CH$_3$), δ = 2.29 ppm (m, –CH–), δ = 4.44 (s, –CH, Fc), δ = 4.53 (s, –CH, Fc). $^{13}C\{^1H\}$, δ = 20.59 ppm (m, –CH$_3$), δ = 21.44 ppm (–CH–), δ = 72.48 ppm (–CH–, Fc), δ = 75.19 ppm (–CH–, Fc). IR (ATR-neat): 2958–2866 cm^{-1} (–C–H alkyl), 1431 cm^{-1} (N–O asym), 1286 cm^{-1} (N–O sym), 1024 cm^{-1} (Fc), 820 cm^{-1} (Fc). Anal. Calcd. for $C_{22}H_{36}O_3NP_2FeCu$: %C,48.59, %H, 6.67, %N, 2.58. Found: %C, 50.22, %H, 6.81, %N, 3.11. Melting Point: 183 °C (d).

X-ray structure determination

Suitable single crystals of compounds (**2**), (**3**), and (**5**) were mounted on a glass fiber, and crystallographic data were collected with an Oxford Diffraction Gemini Atlas diffractometer with a CCD area detector and radiation using a monochromator of graphite with $\lambda_{MoK\alpha}$ = 0.71073 Å at 130 K. Unit cell parameters were determined with a set of three runs of 15 frames (1° in ω). The double-pass method of scanning was used to exclude any noise. The collected frames were integrated by using an orientation matrix determined from the narrow frame scans. CrysAlisPro and CrysAlisRED software packages[51] were used for data collection and integration. Analysis of the integrated data did not reveal any decay. Collected data were corrected for absorption effects by an analytical numeric absorption correction using a multifaceted crystal model based on expressions upon the Laue symmetry with equivalent reflections. Structure solution and refinement were done with SHELXS-2014 (ref. 52) and SHELXL-2014, respectively.[53] WinGX v2023 (ref. 54) software was used to prepare material for publication. Full-matrix least-squares refinement was done by minimizing $(F_o^2 - F_c^2)^2$. All nonhydrogen atoms were refined anisotropically. Hydrogen atoms attached to carbon atoms were placed in geometrically idealized positions and refined as riding on their parent atoms, with C–H = 0.95–1.00 Å with $U_{iso}(H)$ = $1.2U_{eq}(C)$ for aromatic, methine and methylene groups, and $U_{iso}(H)$ = $1.5U_{eq}(C)$ for methyl groups. For compound **5**, attempts made to model the solvent molecule were not successful; the SQUEEZE[55] option in PLATON indicated that there was a large solvent cavity of 185 Å^3. In the final refinement cycles, this contribution of 58 electrons to the electron density was removed from the observed data. For the electron density, the $F(000)$ value in the molecular weight

and the formula are given without considering the results obtained with SQUEEZE. Crystal data and experimental details of compounds (**2**), (**3**), and (**5**) are listed in Tables S25, S27, and S29.†

Data availability

All data are included in the ESI† or available on request.

Conflicts of interest

The authors have no conflicts to declare.

References

1 N. US Department of Commerce, Global Monitoring Laboratory – Carbon Cycle Greenhouse Gases, **https://gml. noaa.gov/ccgg/trends/**, (accessed September 28, 2023).

2 C. Hepburn, E. Adlen, J. Beddington, E. A. Carter, S. Fuss, N. Mac Dowell, J. C. Minx, P. Smith and C. K. Williams, *Nature*, 2019, **575**, 87–97.

3 A. Sobkowiak, D. T. Sawyer and J. L. Roberts, *Electrochemistry for Chemists*, Wiley, 2nd edn, 1995.

4 N. Elgrishi, K. J. Rountree, B. D. McCarthy, E. S. Rountree, T. T. Eisenhart and J. L. Dempsey, *J. Chem. Educ.*, 2018, **95**, 197–206.

5 E. E. Benson, C. P. Kubiak, A. J. Sathrum and J. M. Smieja, *Chem. Soc. Rev.*, 2008, **38**, 89–99.

6 R. Francke, B. Schille and M. Roemelt, *Chem. Rev.*, 2018, **118**, 4631–4701.

7 H. Fujiwara and T. Nonaka, *JEAC*, 1992, **332**, 303–307.

8 Y. Kushi, H. Nagao, T. Nishioka, K. Isobe and K. Tanaka, *J. Chem. Soc., Chem. Commun.*, 1995, 1223–1224.

9 K. Tanaka, Y. Kushi, K. Tsuge, K. Toyohara, T. Nishioka and K. Isobe, *Inorg. Chem.*, 1998, **37**, 120–126.

10 M. M. Ali, H. Sato, T. Mizukawa, K. Tsuge, M. Haga and K. Tanaka, *Chem. Commun.*, 1998, 249–250.

11 M. Rudolph, S. Dautz and E.-G. Jäger, *J. Am. Chem. Soc.*, 2000, **122**, 10821–10830.

12 S.-N. Pun, W.-H. Chung, K.-M. Lam, P. Guo, P.-H. Chan, K.-Y. Wong, C.-M. Che, T.-Y. Chen and S.-M. Peng, *J. Chem. Soc., Dalton Trans.*, 2002, 575–583.

13 R. Angamuthu, P. Byers, M. Lutz, A. L. Spek and E. Bouwman, *Science*, 2010, **327**, 313–315.

14 M. Y. Udugala-Ganehenege, N. M. Dissanayake, Y. Liu, A. M. Bond and J. Zhang, *Transition Met. Chem.*, 2014, **39**, 819–830.

15 C.-J. Huang, Y.-C. Hsu, K. N. Shitaw, Y.-J. Siao, S.-H. Wu, C.-H. Wang, W.-N. Su and B. J. Hwang, *ACS Appl. Mater. Interfaces*, 2022, **14**, 26724–26732.

16 A. Rudie and P. Hart, *Solutions : for people, processes and paper*, 2005, pp. 45–46.

This journal is © The Royal Society of Chemistry 2024

Catal. Sci. Technol., 2024, **14**, 5394–5404 | **5403**

17 Escitalopram Oxalate, https://dailymed.nlm.nih.gov/dailymed/fda/fdaDrugXsl.cfm?setid=ce8be2b4-1525-4864-99c1-9e24815957dc&type=display, (accessed March 28, 2024).

18 H. Sawada and T. Murakami, in *Kirk-Othmer Encyclopedia of Chemical Technology*, 2000.

19 P. Karagiannidis, P. Aslanidis, S. Papastefanou, D. Mentzafos, A. Hountas and A. Terzis, *Inorg. Chim. Acta*, 1989, **156**, 265–270.

20 W. Villarreal, L. Colina-Vegas, G. Visbal, O. Corona, R. S. Corrêa, J. Ellena, M. R. Cominetti, A. A. Batista and M. Navarro, *Inorg. Chem.*, 2017, **56**, 3781–3793.

21 F. G. N. Cloke, V. C. Gibson, M. L. H. Green, V. S. B. Mtetwa and K. Prout, *J. Chem. Soc., Dalton Trans.*, 1988, 2227–2229.

22 H. J. Gysling and G. J. Kubas, in *Inorganic Syntheses*, John Wiley & Sons, Ltd, 1979, pp. 92–97.

23 L. C. Baldwin and M. J. Fink, *J. Organomet. Chem.*, 2002, **646**, 230–238.

24 L. R. Doyle, A. Heath, C. H. Low and A. E. Ashley, *ASC*, 2014, **356**, 603–608.

25 T. Sixt, M. Sieger, M. J. Krafft, D. Bubrin, J. Fiedler and W. Kaim, *Organometallics*, 2010, **29**, 5511–5516.

26 U. K. Komarnicka, S. Kozieł, P. Zabierowski, R. Kruszyński, M. K. Lesiów, F. Tisato, M. Porchia and A. Kyzioł, *J. Inorg. Biochem.*, 2020, **203**, 110926.

27 L. Yang, D. R. Powell and R. P. Houser, *Dalton Trans.*, 2007, 955–964.

28 C. Costentin, S. Drouet, M. Robert and J.-M. Savéant, *Science*, 2012, **338**, 90–94.

29 A. Kütt, S. Tshepelevitsh, J. Saame, M. Lõkov, I. Kaljurand, S. Selberg and I. Leito, *Eur. J. Org. Chem.*, 2021, **2021**, 1407–1419.

30 C. Amatore and J. M. Saveant, *J. Am. Chem. Soc.*, 1981, **103**, 5021–5023.

31 T. A. Shippey, *J. Mol. Struct.*, 1980, **63**, 157–166.

32 H. A. Schwarz and R. W. Dodson, *J. Phys. Chem.*, 1989, **93**, 409–414.

33 J. Schneider, H. Jia, J. T. Muckerman and E. Fujita, *Chem. Soc. Rev.*, 2012, **41**, 2036–2051.

34 S. H. Babcock Jr. , H. P. Lankelma and E. Vopicka, in *Inorganic Syntheses*, John Wiley & Sons, Ltd, 1939, pp. 10–11.

35 What is EPR?, https://sites.cns.utexas.edu/epr_facility/what-epr, (accessed November 9, 2023).

36 A. P. Hunt, A. E. Batka, M. Hosseinzadeh, J. D. Gregory, H. K. Haque, H. Ren, M. E. Meyerhoff and N. Lehnert, *ACS Catal.*, 2019, **9**, 7746–7758.

37 S. Shibata and K. Iijima, *J. Mol. Struct.*, 1984, **117**, 45–50.

38 R. E. LaVilla and S. H. Bauer, *J. Am. Chem. Soc.*, 1963, **85**, 3597–3600.

39 D. A. Roa and J. J. Garcia, *New J. Chem.*, 2023, **47**, 4504–4509.

40 C. De La Cruz and N. Sheppard, *Spectrochim. Acta, Part A*, 2011, **78**, 7–28.

41 L. C. Portis, V. V. Bhat and C. K. Mann, *J. Org. Chem.*, 1970, **35**, 2175–2178.

42 A. Adenier, M. M. Chehimi, I. Gallardo, J. Pinson and N. Vilà, *Langmuir*, 2004, **20**, 8243–8253.

43 D. A. Morgenstern, R. E. Wittrig, P. E. Fanwick and C. P. Kubiak, *J. Am. Chem. Soc.*, 1993, **115**, 6470–6471.

44 M. Marx, H. Frauendorf, A. Spannenberg, H. Neumann and M. Beller, *JACS Au*, 2022, **2**, 731–744.

45 Z. Liu, L.-F. Wu, C. L. Kufner, D. D. Sasselov, W. W. Fischer and J. D. Sutherland, *Nat. Chem.*, 2021, **13**, 1126–1132.

46 C. Costentin, G. Passard and J.-M. Savéant, *J. Am. Chem. Soc.*, 2015, **137**, 5461–5467.

47 D.-M. Feng, Y.-P. Zhu, P. Chen and T.-Y. Ma, *Catalysts*, 2017, **7**, 373.

48 E. S. Rountree, B. D. McCarthy, T. T. Eisenhart and J. L. Dempsey, *Inorg. Chem.*, 2014, **53**, 9983–10002.

49 C. Costentin, S. Drouet, M. Robert and J.-M. Savéant, *J. Am. Chem. Soc.*, 2012, **134**, 19949–19950.

50 W. Yao, A. R. Armstrong, X. Zhou, M.-T. Sougrati, P. Kidkhunthod, S. Tunmee, C. Sun, S. Sattayaporn, P. Lightfoot, B. Ji, C. Jiang, N. Wu, Y. Tang and H.-M. Cheng, *Nat. Commun.*, 2019, **10**, 3483.

51 *CrysAlis-PRO and CrysAlis-RED Agilent Technologies*, Agilent, Yarton, England, 2013.

52 G. M. Sheldrick, *Acta Crystallogr., Sect. A: Found. Adv.*, 2015, **71**, 3–8.

53 G. M. Sheldrick, *Acta Crystallogr., Sect. C: Struct. Chem.*, 2015, **71**, 3–8.

54 L. J. Farrugia, *J. Appl. Crystallogr.*, 2012, **45**, 849–854.

55 A. L. Spek, *Acta Crystallogr., Sect. C: Struct. Chem.*, 2015, **71**, 9–18.

5404 | *Catal. Sci. Technol.*, 2024, **14**, 5394–5404

This journal is © The Royal Society of Chemistry 2024